THE PROTEIN SOCIETY

PROTEIN STRUCTURE REPORT

Crystal structure of the Alpha subunit PAS domain from soluble guanylyl cyclase

Rahul Purohit, Andrzej Weichsel, and William R. Montfort*

Department of Chemistry and Biochemistry, University of Arizona, Tucson, Arizona 85721

Received 7 June 2013; Revised 31 March 2013; Accepted 5 August 2013
DOI: 10.1002/pro.2331
Published online 12 August 2013 proteinscience.org

Abstract: Soluble guanylate cyclase (sGC) is a heterodimeric heme protein of ~150 kDa and the primary nitric oxide receptor. Binding of NO stimulates cyclase activity, leading to regulation of cardiovascular physiology and providing attractive opportunities for drug discovery. How sGC is stimulated and where candidate drugs bind remains unknown. The α and β sGC chains are each composed of Heme-Nitric Oxide Oxygen (H-NOX), Per-ARNT-Sim (PAS), coiled-coil and cyclase domains. Here, we present the crystal structure of the α_1 PAS domain to 1.8 Å resolution. The structure reveals the binding surfaces of importance to heterodimer function, particularly with respect to regulating NO binding to heme in the β_1 H-NOX domain. It also reveals a small internal cavity that may serve to bind ligands or participate in signal transduction.

Keywords: nitric oxide; soluble guanylate cyclase; per-ARNT-sim domain; YC-1; X-ray crystallography; *Manduca sexta*

Introduction

Nitric oxide (NO) is produced in most mammalian cells and serves to regulate blood pressure, wound healing, memory formation, and numerous other physiological processes.[1] The NO receptor is soluble guanylyl/guanylate cyclase (sGC), a large heterodimeric heme protein that is increasingly targeted for drug discovery in the treatment of cardiovascular disease.[2] Two classes of compounds targeting sGC are now in clinical trial, one that stimulates the heme-containing protein (BAY 63-2521/riociguat),[3,4] and another that functions to replace heme after loss due to oxidation (BAY 58-2667/cinaciguat and HMR1766/ataciguat).[5,6] How NO or drug binding leads to cyclase stimulation and signal transduction in sGC is poorly understood.

sGC is composed of two homologous subunits, α and β. Multiple isoforms of each subunit have been identified; however, the most common isoform is the α_1/β_1 heterodimer.[7] Each sGC subunit consists of four domains, an N-terminal Heme-Nitric Oxide Oxygen (H-NOX) domain[8] (also called a SONO domain),[9] a central Per-ARNT-Sim (PAS) domain,[10] a coiled-coil domain and a C-terminal catalytic cyclase domain.[11] NO binding to the heme in the

Abbreviations: H-NOX domain, heme-nitric oxide/oxygen binding domain; PAS domain, Per-ARNT-Sim domain; SAXS, small angle X-ray scattering; sGC, soluble guanylyl cyclase; *Ms* sGC, *Manduca sexta* sGC; *Ms* sGC-NT, *Manduca sexta* sGC lacking the catalytic domains.

Grant sponsor: National Institutes of Health; Grant numbers: HL062969 and U54 CA143924 (to WRM) and S10 RR025485-01A1 (to AW). Grant sponsor: American Heart Association; Grant number: 11PRE7610113 (to RP).

*Correspondence to: William R. Montfort, Department of Chemistry and Biochemistry, The University of Arizona, 1041 E. Lowell St., Tucson, AZ 85721. E-mail: montfort@email.arizona.edu

β_1-subunit leads to the formation of a pentacoordinated Fe–NO complex, stimulation of cyclase activity and production cGMP from GTP. Structural insight into the allostery underlying stimulation is lacking. Structures of individual sGC domains such as the β_1 coiled-coil homodimer[12] and the α_1/β_1 heterodimeric cyclase domain[13] have recently been determined, as have bacterial homologues of the H-NOX and PAS domains.[9,14–16] Yet an understanding of how these domains are arranged in the functional NO sensor remains unknown.

To fill this gap, we have developed sGC from *Manduca sexta* (tobacco hornworm) for biophysical and biochemical characterization.[17–20] *Manduca sexta* sGC (*Ms* sGC) is highly homologous to its mammalian counterparts and responds well to YC-1, the parent compound for riociguat. Using homology modeling, small angle X-ray scattering (SAXS) and chemical cross-linking, we previously determined that *Ms* sGC lacking the cyclase domains (*Ms* sGC-NT) is an elongated molecule with a central parallel coiled-coil.[20] In this model, the α_1 subunit PAS domain directly contacts the heme-containing β_1 subunit H-NOX domain[20] and inhibits NO and CO binding.[1] Here, we present the 1.8 Å crystal structure of the *Ms* sGC α_1 PAS domain, which reveals the H-NOX binding surface and a small internal cavity.

Table I. *Crystallographic Data*

Data measurement	
PDB entry	4GJ4
Wavelength (Å)	0.97950
Space group	H32
Unit cell parameters	$a = b = 95.42$ Å, $c = 317.69$ Å, $\alpha = \beta = 90°$, $\gamma = 120°$
Resolution (Å)[a]	23.7–1.8 (1.86–1.80)
Total reflections	455433 (43841)
Unique reflections	52047 (5122)
Completeness (%)	100.0 (100.0)
Mean I/σ_I	11.3 (1.9)
Redundancy	8.75 (8.56)
R_{merge} (%)	5.5 (69.1)
Refinement	
R_{work} (%)	19.6 (39.8)
R_{free} (%)[b]	24.2 (42.1)
RMS deviation	
Bond lengths (Å)	0.012
Bond angles (°)	1.55
No. of solvent molecules	176
Ramachandran plot	
Most favored (%)	89.9
Allowed (%)	10.1

[a] Overall (outermost shell).
[b] Five percent of data not used in refinement.

Results

Crystal structure of the α_1 PAS domain

Ms sGC α_1 PAS protein was obtained from an *Escherichia coli* expression vector as a SUMO-tagged fusion protein. SUMO cleavage and purification yielded 2–3 mg of highly pure α_1 PAS protein per liter of cell culture. Crystals of the wild-type α_1 PAS domain (residues 279–404) were initially small and could not be improved, possibly due to a requirement for cysteine modification by the arsenic in the cacodylate-containing crystallization buffer.[21–23] To overcome this, we made the triple cysteine mutant C285A, C352A, C374A. This protein crystallized under new conditions, yielding larger crystals with a rhombic dodecahedron morphology and diffraction to 1.8 Å resolution (Table I). Structure solution was by molecular replacement, using the *Nostoc punctiforme* signal transduction histidine kinase (*Np* STHK) PAS domain structure (PDB entry 2P04).[15] Four nearly-identical copies of the α_1 PAS domain were present in the asymmetric unit and were generally well ordered except for the loop between beta strands 4 and 5 (residues 357–361; also called Gβ and Hβ, Fig. 1) and the C-termini. All four C-termini were disordered and not included in the final refined models. In the final model, chains A and C included residues 279–391, chain B included residues 279–390 and chain D included residues 279–395.

The *Ms* sGC α_1 PAS domain contains a typical PAS fold but one that is modified near the site where ligands often bind in PAS-containing proteins (Fig. 1).[10] The core PAS fold consists of a five-stranded antiparallel beta-sheet with strands arranged in the sequence with order 2-1-5-4-3.[10] The segment connecting strand 1 (also called Bβ, Fig. 1) to strand 5 (Gβ) is quite variable both in length and structure among PAS proteins and often provides a ligand-binding surface. Ligands commonly bind in a pocket formed between the beta 1–5 connecting strand and the interior face of the curved beta sheet. An N-terminal flanking helix is generally also present in PAS-containing proteins.

In α_1 PAS, the beta 1–5 connecting strand displays a unique structure as compared with other PAS domains. In most PAS proteins, this segment includes four helices, generally referred to as Cα, Dα, Eα, and Fα. All four helices are present in *Ms* sGC α_1 PAS; however, the residues that form the first half of Fα in a typical PAS domain are seen to form a new beta strand in α_1 PAS (referred to as Fβ in Fig. 1), yielding an overall 6-stranded beta sheet

[1]Rahul Purohit, Bradley Fritz, Juliana The, Aaron Issaian, Andrzej Weichsel, Cynthia David, Eric Campbell, Andrew C. Hausrath, Leida Rassouli-Taylor, Elsa D. Garcin, Matthew J. Gage, and William R. Montfort, *YC-1 Binding to the Beta Subunit of Soluble Guanylyl Cyclase Overcomes Allosteric Inhibition by the Alpha Subunit, in revision.*

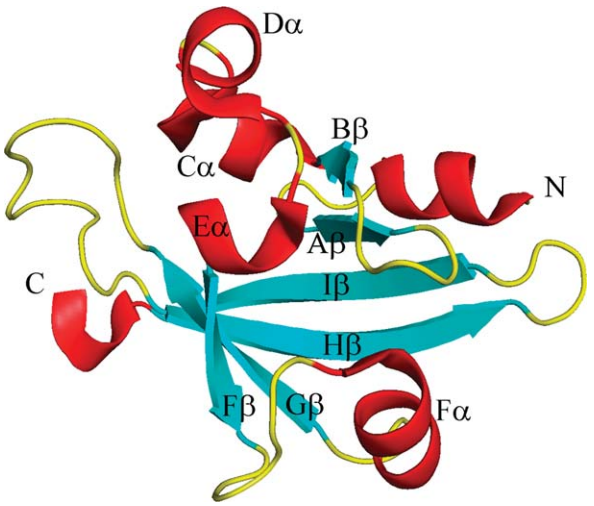

Figure 1. Ribbon diagram of *Ms* sGC α_1 PAS highlighting secondary structure elements. Helix Fα, which splits into a β strand and α helix as compared with canonical PAS domains, is shown as Fβ and Fα.

with topology 2-1-6-5-4-3. The remaining portion of Fα is in a different orientation than typically observed in PAS domains and makes a critical contact with the β_1 H-NOX domain, based on cross-linking studies.[20] The helix includes residues Glu 340 and Lys 343, each of which can be cross-linked to β_1 H-NOX residue Lys 170,[20] indicating that the α_1 PAS and β_1 H-NOX domains are in direct contact in sGC.

Of additional interest is an internal cavity found directly behind the Fα helix in the α_1 PAS structure (Fig. 2). This cavity is in a similar position to the ligand-binding site in other PAS domains, overlapping, for example, with the positions for heme in FixL[24,25] and flavin in the FMN containing LOV domains.[26,27] The cavity size is ~36 Å,^{3} about two-thirds the size of a benzene ring. While it is tempting to suggest this cavity represents a ligand or protein binding site, a substantial rearrangement in the Fα helix would be required to accommodate anything larger than 3–4 atoms. Nonetheless, large rearrangements are known to occur in other PAS domains leading to ligand binding (see, for example, references[28,29]) and the cavity found in *Ms* sGC α_1 PAS may yet have a ligand-binding function. YC-1 appears, however, not to bind to α_1 PAS, but rather to bind to the β_1 H-NOX domain (see footnote *).

The four copies of α_1 PAS in the asymmetric unit are quite similar, displaying similar internal cavity volumes and pairwise RMS deviations in Cα positions of 0.4–0.6 Å. Superpositioning of *Ms* sGC α_1 PAS with *Np* STHK, which was used for molecular replacement, leads to an RMSD of 1.4 Å for 93 core residues (29% identity) when aligned using secondary structure matching (SSM).[30] Superimposing *Ms* sGC α_1 PAS with heme-containing FixL (PDB entry 1EW0)[25] and FAD-containing PAS1 of NIFL (PDB entry 2GJ3)[26] reveal RMSD values of 2.7 Å for 87 core residues (10% identity) and 2.7 Å for 86 core residues (11% identity), respectively. The key difference between the FixL and NIFL PAS1 structures is the position of the Fα helix.

Discussion

The α_1 PAS crystal structure provides constraints for understanding domain arrangement in sGC. The overall fold is typical for PAS domains but displays a unique arrangement for the most variable region in the family, the segment connecting beta sheet strands 1 and 5. In this segment, the Fα helix is split into a sixth beta strand and a shorter helix with a new orientation with respect to most other PAS domains, but similar to that of *Np* STHK.[15]

In *Ms* sGC-NT, a parallel coiled-coil provides a platform on which the other domains assemble.

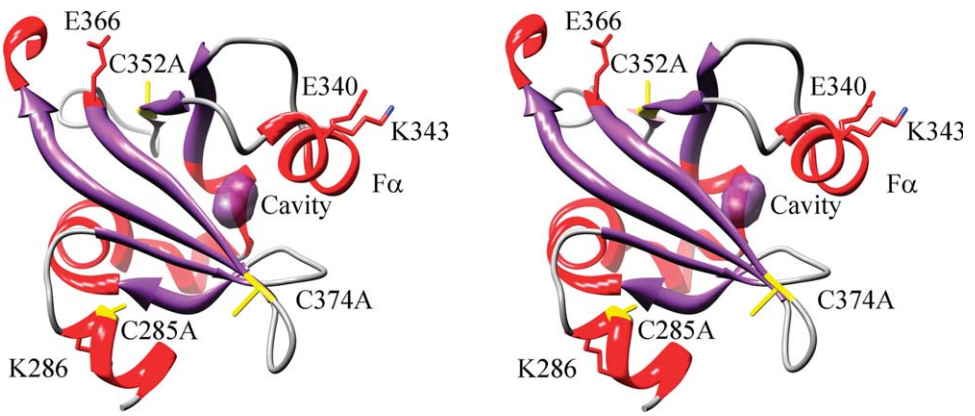

Figure 2. Ribbon drawing of *Ms* sGC α_1 emphasizing the small internal pocket and inter-domain contact residues (cross-eyed stereo view). The small internal pocket found in the structure is highlighted in purple and the C285A, C352A, C374A mutations are shown in yellow. Also shown are residues Glu 340 and Lys 343, which can be cross-linked to the β_1 H-NOX domain; residue Lys 286, which can be cross-linked to the β_1 PAS domain; and residue Glu 366, which can be cross-linked to the β_1 coiled-coil.

Direct cross-links between the α_1 PAS Fα helix and the β_1 H-NOX domain near the heme pocket suggest the two domains are in direct contact, providing a means for allosteric regulation of the protein. Both domains also cross-link with the coiled-coil domain. Our working hypothesis is that YC-1 binding disrupts the α_1 PAS/β_1 H-NOX interaction, leading to a closed H-NOX domain and tighter CO and NO binding.

PAS domains often form homo- or hetero-oligomers as part of their function[10] and the possibility that sGC forms an α_1/β_1 PAS dimer has been previously proposed. The most compelling data are based on the oligomer formed by *Np* STHK, which shares sequence homology with the sGC PAS domains.[15] *Np* STHK forms a homodimer involving a hydrophobic patch near the N-terminus and a strand swap that allows Leu 8 from one chain to cover the hydrophobic patch of the other chain in the dimer. Several hydrogen bonds help stabilize the dimer while removal of the first seven residues in the protein abolishes the dimer. Intriguingly, the rat β_1 PAS domain also dimerizes. In contrast, our construct for *Ms* α_1 PAS runs as a monomer over a sizing column and appears to be monomeric in solution. The protein crystallizes as a rhombic dodecahedron, but this arrangement is likely an artifact of crystallization and of no physiological significance. The N-terminal hydrophobic patch at the heart of the *Np* STHK dimer interface is also found in *Ms* α_1 PAS; however, it does not lead to a dimer interface. Our structure is six residues shorter at the N-terminus than that for the rat β_1 PAS construct and, conceivably, this could alter dimer formation much as it did in *Np* STHK. Nonetheless, our cross-linking data for *Ms* sGC-NT include a link between α_1 Lys 286 and β_1 Glu 196, located at the N-termini of the two PAS domains, indicating the two PAS domains are in contact in the intact heterodimer.[20]

The *Ms* sGC α_1 PAS structure also displays a small internal cavity behind the Fα helix (Fig. 2). Our binding data indicate YC-1 does not bind to this domain but do not rule out another role for this pocket in ligand binding. For ligand binding to occur, the beta 1–5 connecting segment, which includes the Fα helix, would need to rearrange, allowing the pocket to open up. There is precedent for such rearrangements in PAS domain proteins. For example, human PAS kinase has a dynamic Fα helix in the PAS A domain that allows for small molecule entry into the hydrophobic protein core, near to where the internal cavity lies in sGC α_1 PAS.[28] Importantly, the ligand-binding pocket is collapsed in the apo protein and only forms upon ligand binding. A second example is that of histidine kinase CitA, which uses a PAS domain for sensing citrate.[29] In CitA, the beta 1–5 connecting segment is poorly ordered in the absence of citrate binding, but becomes well ordered in the complex with citrate bound in the protein interior. The loop connecting beta strands 4 and 5 also rearranges upon citrate binding, shifting inward. In *Ms* sGC α_1 PAS, the beta 4–5 loop is poorly ordered and could serve a similar role in ligand binding or in signal transduction.

Materials and Methods

Ms sGC α_1 PAS expression and purification

All chemicals were obtained from Sigma-Aldrich, restriction enzymes from New England Biolabs, and purification columns from GE Healthcare unless otherwise indicated. *Ms* sGC α_1 PAS with a N-terminal His-tagged SUMO fusion was cloned into the pETH-SUL vector,[31] expressed in *E. coli* strain BL21 (DE3) pLysS, and purified after cleavage of the SUMO tag with SUMO hydrolase, as described elsewhere (see footnote *). The final material was concentrated to 10–15 mg/mL using a Vivaspin concentrator (Sartorius Stedim Biotech) and stored at –80°C. A final yield 2–3 mg of highly pure protein was obtained per liter of cell culture.

Crystallization

Initial crystallization conditions for *Ms* sGC α_1 PAS were found using a PHOENIX protein crystallization robot (Art Robbins Instruments) and commercially available screens (Hampton Research and Qiagen). Crystals formed in a 96-well Intelli-Plate using sitting drop vapor diffusion at 4°C and precipitants of 1.4–1.6 *M* ammonium sulfate, 50 m*M* sodium cacodylate (pH 5.5–6.5) and 15 m*M* magnesium acetate tetrahydrate. Protein at 10–15 mg/mL was mixed with precipitant at ratios of 1:1 and 1:2. Cubic crystals appeared within 24–48 h after plate setup but failed to grow beyond 100 μm in size. Diffraction quality hexagonal crystals for *Ms* sGC P35α (cysteine triple mutant) were obtained by hanging drop vapor diffusion at 4°C using a precipitant solution of 1.5 *M* lithium sulfate, 0.1 *M* Hepes (pH 7.5). Small crystals were also observed from 4.3 *M* NaCl, 0.1 *M* Hepes (pH 7.5) and from 25% PEG 3350, 0.2 *M* NaCl, 0.1 *M* Hepes (pH 7.5). Total of 90% saturated lithium sulfate was used as the cryoprotectant and crystals were flash frozen in liquid nitrogen.

Data collection, structure solution, and refinement

X-ray diffraction data for *Ms* sGC α_1 PAS (wild type) cubic crystals were measured remotely on SSRL beamline 9–2 (Stanford) using a MAR325 detector at T = 100 K and λ = 0.97950 Å. The data were processed in space group $P2_13$ to 3.7 Å resolution using CrystalClear.[32] The unit cell parameters were $a = b = c$ = 143.26 Å, and $\alpha = \beta = \gamma = 90°$.

Diffraction data for hexagonal crystals of *Ms* sGC α_1 PAS (triple mutant) were also measured remotely on SSRL beamline 7-1 (Stanford) using a MAR325 detector at T = 100 K, λ = 0.97950 Å and were processed to 1.8 Å with CrystalClear in hexagonal space group H32 (Table I). There were four molecules in the asymmetric unit. The structure was determined using molecular replacement as implemented in MrBUMP[33,34] and search models generated from the structure of the *Nostoc punctiforme* signal transduction histidine kinase HNOXA domain (PDB entries 2P04 and 2P08),[15] which yielded an ensemble model. Model building and refinement were performed using programs COOT and REFMAC5.[35,36] Figures were prepared using PyMOL (W. L. DeLano, http://www.pymol.org) and UCSF Chimera.[37] Model quality was evaluated with PROCHECK.[38] Cavity volume was computed using CASTp.[39]

Atomic Coordinates

The atomic coordinates and structure factors have been deposited with the Protein Data Bank (PDB entry 4GJ4).

Acknowledgments

Portions of this research were carried out at the Stanford Synchrotron Radiation Lightsource, a national user facility operated by Stanford University on behalf of the USA Department of Energy, Office of Basic Energy Sciences. The SSRL Structural Molecular Biology Program is supported by the Department of Energy, Office of Biological and Environmental Research, and by the National Institutes of Health, National Center for Research Resources, Biomedical Technology Program, and the National Institute of General Medical Sciences. Molecular graphics and analyses were performed with the UCSF Chimera package. Chimera is developed by the Resource for Biocomputing, Visualization, and Informatics at the University of California, San Francisco (supported by NIGMS P41-GM103311).

References

1. Ignarro LJ, editor (2010) Nitric Oxide Biology and Pathobiology. Second ed. San Diego: Academic Press.
2. Evgenov OV, Pacher P, Schmidt PM, Hasko G, Schmidt HH, Stasch JP (2006) NO-independent stimulators and activators of soluble guanylate cyclase: discovery and therapeutic potential. Nat Rev Drug Discov 5:755–768.
3. Belik J (2009) Riociguat, an oral soluble guanylate cyclase stimulator for the treatment of pulmonary hypertension. Curr Opin Investig Drugs 10:971–979.
4. Mittendorf J, Weigand S, Alonso-Alija C, Bischoff E, Feurer A, Gerisch M, Kern A, Knorr A, Lang D, Muenter K, Radtke M and others (2009) Discovery of riociguat (BAY 63-2521): a potent, oral stimulator of soluble guanylate cyclase for the treatment of pulmonary hypertension. ChemMedChem 4:853–865.
5. Schmidt PM, Schramm M, Schroder H, Wunder F, Stasch JP (2004) Identification of residues crucially involved in the binding of the heme moiety of soluble guanylate cyclase. J Biol Chem 279:3025–3032.
6. Schindler U, Strobel H, Schonafinger K, Linz W, Lohn M, Martorana PA, Rutten H, Schindler PW, Busch AE, Sohn M, Topfer A and others (2006) Biochemistry and pharmacology of novel anthranilic acid derivatives activating heme-oxidized soluble guanylyl cyclase. Mol Pharmacol 69:1260–1268.
7. Derbyshire ER, Marletta MA (2012) Structure and regulation of soluble guanylate cyclase. Annu Rev Biochem 81:533–559.
8. Cary SP, Winger JA, Derbyshire ER, Marletta MA (2006) Nitric oxide signaling: no longer simply on or off. Trends Biochem Sci 31:231–239.
9. Nioche P, Berka V, Vipond J, Minton N, Tsai AL, Raman CS (2004) Femtomolar sensitivity of a NO sensor from Clostridium botulinum. Science 306:1550–1553.
10. Moglich A, Ayers RA, Moffat K (2009) Structure and signaling mechanism of Per-ARNT-Sim domains. Structure 17:1282–1294.
11. Liu Y, Ruoho AE, Rao VD, Hurley JH (1997) Catalytic mechanism of the adenylyl and guanylyl cyclases: modeling and mutational analysis. Proc Natl Acad Sci USA 94:13414–13419.
12. Ma X, Beuve A, van den Akker F (2010) Crystal structure of the signaling helix coiled-coil domain of the beta1 subunit of the soluble guanylyl cyclase. BMC Struct Biol 10:2.
13. Allerston CK, von Delft F, Gileadi O (2013) Crystal structures of the catalytic domain of human soluble guanylate cyclase. PLoS One 8:e57644.
14. Pellicena P, Karow DS, Boon EM, Marletta MA, Kuriyan J (2004) Crystal structure of an oxygen-binding heme domain related to soluble guanylate cyclases. Proc Natl Acad Sci USA 101:12854–12859.
15. Ma X, Sayed N, Baskaran P, Beuve A, van den Akker F (2008) PAS-mediated dimerization of soluble guanylyl cyclase revealed by signal transduction histidine kinase domain crystal structure. J Biol Chem 283: 1167–1178.
16. Ma X, Sayed N, Beuve A, van den Akker F (2007) NO and CO differentially activate soluble guanylyl cyclase via a heme pivot-bend mechanism. EMBO J 26:578–588.
17. Hu X, Feng C, Hazzard JT, Tollin G, Montfort WR (2008) Binding of YC-1 or BAY 41-2272 to soluble guanylyl cyclase induces a geminate phase in CO photolysis. J Am Chem Soc 130:15748–15749.
18. Hu X, Murata LB, Weichsel A, Brailey JL, Roberts SA, Nighorn A, Montfort WR (2008) Allostery in recombinant soluble guanylyl cyclase from Manduca sexta. J Biol Chem 283:20968–20977.
19. Fritz BG, Hu X, Brailey JL, Berry RE, Walker FA, Montfort WR (2011) Oxidation and loss of heme in soluble guanylyl cyclase from Manduca sexta. Biochemistry 50:5813–5815.
20. Fritz BG, Roberts SA, Ahmed A, Breci L, Li W, Weichsel A, Brailey JL, Wysocki VH, Tama F, Montfort WR (2013) Molecular model of a soluble guanylyl cyclase fragment determined by small-angle x-ray scattering and chemical cross-linking. Biochemistry 52: 1568–1582.
21. Jacobson KB, Murphy JB, Das Sarma B (1972) Reaction of cacodylic acid with organic thiols. FEBS Lett 22:80–82.
22. Maignan S, Guilloteau JP, Zhou-Liu Q, Clement-Mella C, Mikol V (1998) Crystal structures of the catalytic domain of HIV-1 integrase free and complexed with its

metal cofactor: high level of similarity of the active site with other viral integrases. J Mol Biol 282:359–368.
23. Winger JA, Derbyshire ER, Lamers MH, Marletta MA, Kuriyan J (2008) The crystal structure of the catalytic domain of a eukaryotic guanylate cyclase. BMC Struct Biol 8:42.
24. Gong W, Hao B, Mansy SS, Gonzalez G, Gilles-Gonzalez MA, Chan MK (1998) Structure of a biological oxygen sensor: a new mechanism for heme- driven signal transduction. Proc Natl Acad Sci USA 95:15177–15182.
25. Miyatake H, Mukai M, Park SY, Adachi S, Tamura K, Nakamura H, Nakamura K, Tsuchiya T, Iizuka T, Shiro Y (2000) Sensory mechanism of oxygen sensor FixL from Rhizobium meliloti: crystallographic, mutagenesis and resonance Raman spectroscopic studies. J Mol Biol 301:415–431.
26. Key J, Hefti M, Purcell EB, Moffat K (2007) Structure of the redox sensor domain of Azotobacter vinelandii NifL at atomic resolution: signaling, dimerization, and mechanism. Biochemistry 46:3614–3623.
27. Crosson S, Moffat K (2001) Structure of a flavin-binding plant photoreceptor domain: insights into light-mediated signal transduction. Proc Natl Acad Sci USA 98:2995–3000.
28. Amezcua CA, Harper SM, Rutter J, Gardner KH (2002) Structure and interactions of PAS kinase N-terminal PAS domain: model for intramolecular kinase regulation. Structure 10:1349–1361.
29. Sevvana M, Vijayan V, Zweckstetter M, Reinelt S, Madden DR, Herbst-Irmer R, Sheldrick GM, Bott M, Griesinger C, Becker S (2008) A ligand-induced switch in the periplasmic domain of sensor histidine kinase CitA. J Mol Biol 377:512–523.
30. Krissinel E, Henrick K (2004) Secondary-structure matching (SSM), a new tool for fast protein structure alignment in three dimensions. Acta Crystallogr D Biol Crystallogr 60:2256–2268.
31. Weeks SD, Drinker M, Loll PJ (2007) Ligation independent cloning vectors for expression of SUMO fusions. Protein Expr Purif 53:40–50.
32. Pflugrath JW (1999) The finer things in X-ray diffraction data collection. Acta Crystallogr D55:1718–1725.
33. Keegan RM, Long F, Fazio VJ, Winn MD, Murshudov GN, Vagin AA (2011) Evaluating the solution from MrBUMP and BALBES. Acta Crystallogr D Biol Crystallogr 67:313–323.
34. Keegan RM, Winn MD (2008) MrBUMP: an automated pipeline for molecular replacement. Acta Crystallogr D Biol Crystallogr 64:119–124.
35. Emsley P, Lohkamp B, Scott WG, Cowtan K (2010) Features and development of Coot. Acta Crystallogr D Biol Crystallogr 66:486–501.
36. Murshudov GN, Skubak P, Lebedev AA, Pannu NS, Steiner RA, Nicholls RA, Winn MD, Long F, Vagin AA (2011) REFMAC5 for the refinement of macromolecular crystal structures. Acta Crystallogr D Biol Crystallogr 67:355–367.
37. Pettersen EF, Goddard TD, Huang CC, Couch GS, Greenblatt DM, Meng EC, Ferrin TE (2004) UCSF Chimera – a visualization system for exploratory research and analysis. J Comput Chem 25:1605–1612.
38. Laskowski RA, MacArthur MW, Moss DS, Thorton JM (1993) PROCHECK: A program to check the stereochemical quality of protein structures. J Appl Crystal 26:283–291.
39. Dundas J, Ouyang Z, Tseng J, Binkowski A, Turpaz Y, Liang J (2006) CASTp: computed atlas of surface topography of proteins with structural and topographical mapping of functionally annotated residues. Nucleic Acids Res 34:W116–W118.